

Evidence for a proximity-induced energy gap in Nb/InAs/Nb junctions

A. Chrestin, T. Matsuyama, and U. Merkt

Universität Hamburg, Institut für Angewandte Physik und Zentrum für Mikrostrukturforschung, Jungiusstrasse 11,
D-20355 Hamburg, Germany

(Received 13 September 1996)

We investigate the subharmonic energy gap structure (SGS) in coplanar Nb/*p*-type InAs(2DEG)/Nb junctions. The junctions are produced by employing a technique which enables us to achieve distances between the superconducting electrodes considerably below 100 nm. In the coplanar geometry of our junctions, a smearing of the SGS is expected when a voltage drop along the Nb/InAs interfaces is present. This behavior is indeed observed in junctions with interfaces of minor quality. In junctions with high-quality interfaces, the SGS is well developed despite the coplanar geometry. We interpret the absence of smearing, together with a temperature-dependent shift of the SGS, in terms of a recent theory by Aminov *et al.* Within this theory, the influence of the proximity effect on the InAs inversion layer under the Nb electrodes is taken into account, leading to the opening of a gap in the density of states. Because of the narrow inversion layer and the high interface transparency, the gap is comparable in magnitude to the superconducting energy gap Δ of the Nb. For our junction, we find from the shift of the SGS a gap of 0.81Δ at temperature $T=0$ induced in the inversion layer. [S0163-1829(97)07413-4]

I. INTRODUCTION

Over the past few years, the amount of research devoted to the study of superconductor-semiconductor-superconductor (SSmS) junctions has increased considerably. The main interest for application is focused on three-terminal SSmS weak links, in which the magnitude of the Josephson supercurrent can be controlled externally. In many respects, SSmS devices can usually be regarded as special realizations of superconductor-normal conductor-superconductor (SNS) junctions. It is by now well established that a crucial parameter for the performance of these devices is the SSm interface transparency. For this reason, InAs is a well suited semiconductor material, because due to Fermi-level pinning in the conduction band a Schottky barrier at the interface can be avoided. The high interface transmissivity leads to a large probability of Andreev reflection, a process in which an electron incoming from the normal conductor is reflected as a hole while a Cooper pair is created in the superconductor.¹ The probability of this process largely determines the transport properties of SSmS and SNS junctions. A simple model demonstrating the influence of interface transparency on the I - V curves of SNS junctions has been developed by Octavio, Tinkham, Blonder, and Klapwijk (OTBK).² In this model, the barrier heights at the interfaces sensitively influence the amount of excess current and the magnitude of the subharmonic energy gap structure (SGS). Excess current manifests itself as a positive intercept with the current axis of the linear high-voltage I - V characteristics, extrapolated to zero voltage; it becomes negative (deficit current) when the barrier strength is increased. Subharmonic energy gap structure refers to a modulation of the differential resistance dV/dI at voltages around $2\Delta/ne$, with n an integer and the temperature-dependent energy gap $\Delta(T)$ of the superconductors.

We have produced coplanar SSmS junctions with Nb superconducting electrodes and *p*-type InAs as the semicon-

ductor (see Fig. 1). The weak link is established through the quasi-two-dimensional electron gas (2DEG) in the native inversion layer at the *p*-type InAs surface. By using an anodic oxide film on one of the Nb electrodes as a spacer, we can study junctions with extremely short electrode separation, below the normal coherence length $\xi_N = [\hbar D/2\pi k_B T]^{1/2}$ as well as the elastic and inelastic mean free paths l and l_{in} . Here, $D = v_F l/2$ is the diffusion coefficient, and v_F the Fermi velocity in the inversion layer. In coplanar SSmS junctions realized with an InGaAs heterostructure³ or an InAs inserted channel in an InAlAs/InGaAs heterostructure,⁴ smearing of the energy-dependent features predicted by the OTBK model has been attributed to a potential gradient along the SSm interfaces. We find comparable effects in our junctions. However, after improving the interface quality, these effects are no longer observed. Instead, we find a well developed SGS, but at low temperatures the peaks are shifted to voltages too small to be accounted for by the superconducting energy gap of the Nb electrodes. This can be understood in terms of a proximity-induced coherent state in the part of the inversion layer covered by the superconductor, accompanied by the opening of a gap in the density of states, as first described by McMillan

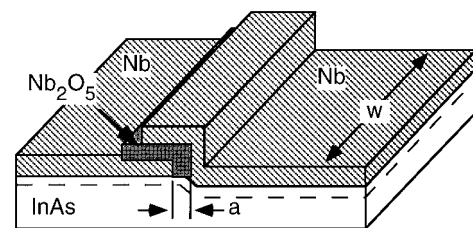


FIG. 1. Sketch of the experimental junction geometry. The broken line indicates the inversion layer at the *p*-type InAs surface, which forms a quasi-two-dimensional electron gas (2DEG) under the niobium oxide.

for an SN sandwich.⁵ We will compare our data to a recent extension of the OTBK model that takes this effect into account within the quasiclassical Green's function theory.⁶

The organization of the paper is as follows. In the following section, the fabrication of our junctions and the experimental setup are described. The theoretical concepts of the OTBK model and the model of Ref. 6 are discussed with respect to our junction geometry in Sec. III. In Sec. IV, we first briefly present the data for one junction showing smearing of the SGS. A detailed discussion of the experimental features of the junctions with high-quality interfaces and a comparison to the theory follows. Finally, a conclusion is given in Sec. V.

II. EXPERIMENTAL DETAILS

The semiconductors are *p*-type InAs wafers with a nominal doping of about $2 \times 10^{17} \text{ cm}^{-3}$. After mechanical and chemical polishing of the sample, the first Nb electrode is defined by optical lithography. Immediately afterwards, the sample is inserted into the Nb sputtering chamber. When a base pressure of $< 10^{-8}$ mbar is reached, the vessel is flooded with Ar (10^{-2} mbar) and a three-step sputtering process begins. In the first step, a possibly contaminated surface layer of the Nb target is removed by dc magnetron sputtering. The sputtered Nb also serves to getter some of the remaining oxygen and nitrogen impurities. During this process, the sample is protected by a shutter. In the second step, the sample surface is cleaned by rf sputtering (dc bias ~ 200 V). Finally, the shutter is opened and the Nb film is deposited on the sample again by dc magnetron sputtering. The electrode patterning is completed by a liftoff process after removal of the sample from the sputtering system. Then the part of the sample surface that contains the front edge of the Nb electrode is anodically oxidized to the desired thickness in a solution of 26 g ammonium pentaborate and 187.3 ml ethylene glycol in 126.6 ml water.⁷ Per volt of anodization voltage, an oxide film of approximately 2 nm thickness grows. At the same time, the exposed InAs surface is oxidized. Subsequently, the second Nb electrode and the contact pads are realized by optical lithography as windows in a photoresist mask, the window for the second electrode overlapping the oxide film on the first one for approximately 10 μm . Through the window, the oxidized InAs is removed by wet etching for 1 min in 1:1 $\text{H}_2\text{SO}_4(96\%):\text{H}_2\text{O}$, terminated by rinsing in H_2O . The sulfuric acid does not etch Nb_2O_5 and without oxidizing agent like H_2O_2 nonoxidized InAs is only etched very slowly, so that the process virtually stops as soon as the oxidized InAs is removed. After this etching step, the sample is again inserted as quickly as possible into the sputtering chamber, and the second electrode together with the contact pads are patterned as described above for the first electrode. A schematic view of the completed sample is shown in Fig. 1. The junctions investigated had electrode widths $w = 43$ and $91 \mu\text{m}$ and oxide thicknesses between 20 and 80 nm.

The important improvement in the fabrication process to obtain the high-quality interfaces was a modification of the shutter system that protects the samples during the target cleaning. In the new setup, special care was taken to keep the gap between the shutter and the sample as small as possible

during the target cleaning step. We therefore assume that when a larger gap exists, some Nb can be scattered around the shutter due to frequent collisions with the Ar atoms and is deposited on the sample already before the shutter is opened. The Nb could then easily react, for example, with oxygen during its rather long exposure to the residual atmosphere before being covered by the intentionally deposited film. Junctions produced with the same shutter configuration consistently showed the same qualitative behavior.

It is well known that niobium oxide is not comparable in quality as an insulator to, say, aluminum oxide. In particular, lower oxidation stages than Nb_2O_5 are known to have semiconducting or even superconducting properties.^{8,9} The question therefore arises whether a weak link through the oxide is formed. We can exclude this for different reasons. When the anodic oxide was investigated by x-ray induced photoemission spectroscopy (XPS), the Nb *3d* peak consisted only of an Nb_2O_5 component. After Ar sputter cleaning of the sample, it was found that part of the oxide was reduced to lower oxidation stages, in agreement with previous results of Grundner and Halbritter.¹⁰ To exclude the formation of shorts by the Ar sputtering, we have produced junctions as described above on a semi-insulating Si substrate, but with an overlapping area of $\sim 1 \text{ mm}^2$. Despite of this large area, no weak-link behavior could be detected.

There have been previous investigations on the feasibility of anodic oxidation for the production of tunnel junctions.^{11,12} Aponte *et al.*¹² found that they had to reduce the thickness of the oxide film to 5.5 nm or less by Ar sputter etching to observe Josephson coupling. Because of their high-energy sputtering, formation of lower oxides may have occurred to an even larger extent than could be expected here. Nevertheless, they always observed a *tunnel* junction behavior, unless the oxide thickness was reduced to less than 0.8 nm. In contrast, we observe high-transparency weak-link behavior for oxide thicknesses of 20 nm and more, so that the 2DEG must be responsible for the Josephson coupling. Also the large sensitivity to the interface preparation discussed below would not be expected when the oxide provided the coupling. Finally we want to mention investigations of Fiske steps in our junctions¹³ which are indicative of a confinement of the Josephson coupling to the front edge of the electrodes, as it is expected for coupling through the 2DEG.

The measurements are performed in a conventional liquid-helium cryostat down to temperatures of 1.5 K. When no magnetic field is applied, the samples are protected from external fields by a cryoperm shield. Leads are filtered at room temperature with commercially available filters. All measurements are done in a four-probe setup under current bias. The differential resistance is measured by standard lock-in technique with a modulating current of 1–5 μA at 300 Hz.

III. THEORETICAL CONCEPTS

The appearance of SGS in a SNS junction due to multiple Andreev reflection has originally been explained by Klapwijk *et al.*¹⁴ in a model that does not include normal scattering. Taking up this idea, Octavio *et al.*² calculated the *I-V* characteristics of a ballistic normal-conducting constriction

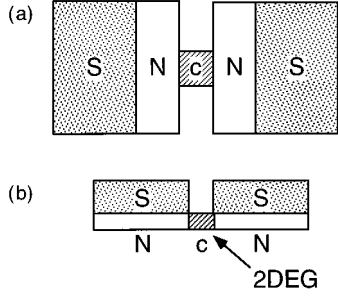


FIG. 2. (a) The geometry assumed in the model of Aminov *et al.* (Ref. 6). The geometry of the OTBK model (Ref. 2) is obtained by reducing the thicknesses of the N layers to zero. (b) Description of the SNcNS system as realized in the experimental junctions of this paper.

sandwiched between two superconductors in a Boltzmann-equation approach. They assumed that the constriction is small enough that neither a deviation of the superconducting electrodes from equilibrium nor a depression of the pair potential near the interfaces by the proximity effect must be taken into account. The pair potential in the constriction is set equal to zero. The only source of scattering are δ -function potential barriers of dimensionless strength Z at the SN interfaces, $V(x) = \hbar v_F Z [\delta(x) + \delta(x-L)]$. The constriction extends between $x=0$ and $x=L$. From the energy-dependent probabilities of Andreev reflection $A(E)$, normal reflection $B(E)$ and transmission $T(E) = 1 - A(E) - B(E)$ of Blonder *et al.*,¹⁵ the voltage-dependent nonequilibrium electron distribution in the constriction is determined. The current is proportional to the energy-integrated difference of the distribution functions of left- and right-running states in the constriction.

Aminov *et al.*⁶ extended the model by taking into account thin normal layers adjacent to the superconductors, as shown in Fig. 2(a). The SN layers are assumed to be in the dirty limit and, as in the OTBK model, to be not disturbed by the current through the constriction c . The equilibrium state of the SN layers is described by the angle-averaged Green's functions G and F , which are obtained from a diffusionlike equation.^{16,17} By formally introducing a complex angle $\theta(\epsilon, x)$ with $G(\epsilon, x) = \cos\theta(\epsilon, x)$ and $F(\epsilon, x) = \sin\theta(\epsilon, x)$, the equation reads

$$\tilde{\xi}_{N,S}^2 \theta''_{N,S}(x) + i\epsilon \sin\theta_{N,S}(x) + \tilde{\Delta}_{N,S}(x) \cos\theta_{N,S}(x) = 0. \quad (1)$$

G and F are the normal and anomalous part of the angle-averaged Green's function, $\epsilon = E/\pi k_B T_c$ and $\tilde{\Delta}_{N,S} = \Delta_{N,S}/\pi k_B T_c$ are the normalized energy and pair potential, and T_c is the critical temperature of the superconductors. The coherence lengths in N and S are given by $\tilde{\xi}_{N,S} = [\hbar D_{N,S}/2\pi k_B T_c]^{1/2}$, with the diffusion coefficients $D_{N,S}$. The pair potential in the normal layers is assumed to be zero. In the superconductors, it is determined by the self-consistency equation

$$\tilde{\Delta}_S(x) \ln \frac{T}{T_c} + 2 \frac{T}{T_c} \sum_{\omega_n > 0} \left[\frac{\tilde{\Delta}_S(x)}{\omega_n} - \sin\theta_S(i\omega_n, x) \right] = 0, \quad (2)$$

where $\omega_n = (2n+1)T/T_c$ are the normalized Matsubara frequencies. Considering one SN double layer with the boundary to the constriction at $x = -d_N$ and the SN interface at $x=0$, Eq. (1) has to be solved subject to the boundary conditions¹⁸

$$\tilde{\gamma}_B \tilde{\xi}_N \theta'_N(0^-) = \sin[\theta_S(0^+) - \theta_N(0^-)], \quad (3a)$$

$$\tilde{\gamma} \tilde{\xi}_N \theta'_N(0^-) = \tilde{\xi}_S \theta'_S(0^+), \quad (3b)$$

$$\theta_S(\infty) = \arctan(i\tilde{\Delta}(T)/\epsilon), \quad (3c)$$

$$\theta'_N(-d_N) = 0. \quad (3d)$$

In these equations, $\tilde{\Delta}$ denotes the normalized value of the pair potential in the bulk superconductor, $\tilde{\gamma} = \rho_S \tilde{\xi}_S / \rho_N \tilde{\xi}_N$ is a parameter characterizing the strength of the proximity effect between S and N and $\tilde{\gamma}_B = R_B / \rho_N \tilde{\xi}_N$ describes the effect of boundary transparency. R_B is the specific boundary resistance, ρ_S and ρ_N are the resistivities of S and N in the normal state. Note that the last boundary condition corresponds to the one at the interface to an insulator, explicitly showing that any influence of the constriction is neglected. The probabilities of Andreev and normal reflection for particles incoming from the constriction are given by^{19,20}

$$A(\epsilon) = \frac{|\sin\theta_N(\epsilon, -d_N)|^2}{|1 + 2Z^2 + \cos\theta_N(\epsilon, -d_N)|^2}, \quad (4)$$

$$B(\epsilon) = \frac{4Z^2(1+Z^2)}{|1 + 2Z^2 + \cos\theta_N(\epsilon, -d_N)|^2}. \quad (5)$$

The model described so far is essentially one-dimensional and not immediately applicable to the geometry of the experimental device depicted in Fig. 2(b). Nevertheless we can expect to get a qualitatively correct picture as will be detailed in the following. As long as the SN layers are only negligibly disturbed by the constriction, the Green's functions can be calculated as above also in the geometry of Fig. 2(b), x now being the vertical coordinate. At $x = -d_N$, the interface between inversion and depletion layers corresponds to the normal conductor/insulator interface. Since the constriction is no longer located at $x = -d_N$, the model only makes sense when a space dependence of the Green's functions in the normal layer can be neglected. This is allowed for $d_N \ll \tilde{\xi}_N$, which is an acceptable approximation since the thickness of the inversion layer is $d_N \approx 10$ nm, whereas $\tilde{\xi}_N \approx 50$ – 100 nm. A further simplification is possible concerning the proximity-effect parameter $\tilde{\gamma}$. Using the relation²¹ $\rho_S l_S = 3.7 \times 10^{-16} \Omega \text{ m}^2$ valid for single-crystal Nb as an estimate, we obtain $\rho_S \tilde{\xi}_S = 6.2 \times 10^{-16} \Omega \text{ m}^2$ with a Fermi velocity $v_F = 6.2 \times 10^5 \text{ m s}^{-1}$ and a mean free path²² $l_S \approx 10$ nm. On the other hand, for typical InAs inversion layer parameters (carrier density $N_S \approx 10^{16} \text{ m}^{-2}$, effective mass $m^* \approx 0.03 m_e$, mean free path $l_N \approx 100$ nm), we have a sheet resistance $R^\square = 1 \text{ k}\Omega$ and $\tilde{\xi}_N = 80$ nm. From these numbers we get $\tilde{\gamma} \approx 10^{-3}$, which means that the inversion layer is very ineffective in suppressing the pair potential in the superconductor due to its low electron density. By setting

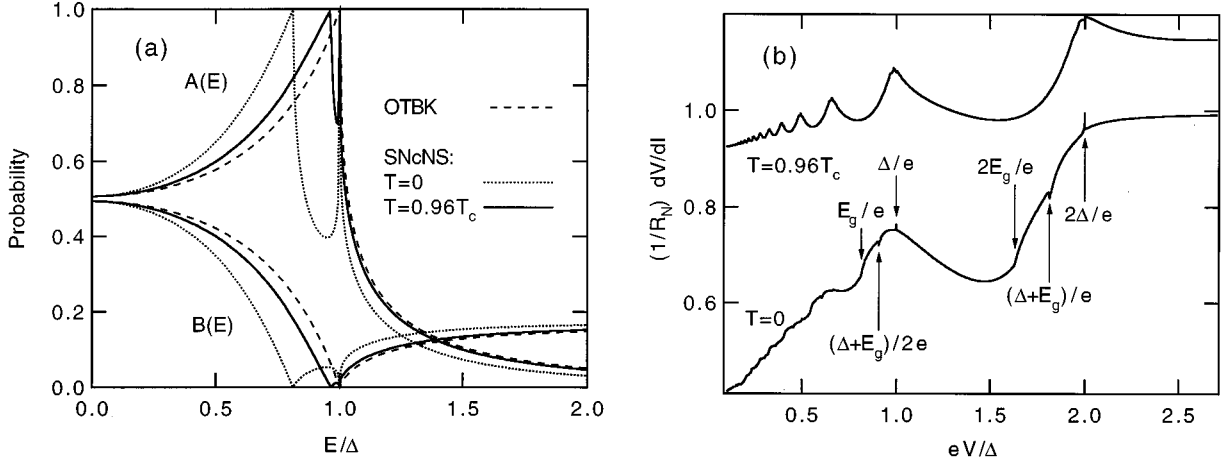


FIG. 3. (a) Andreev and normal reflection probabilities $A(E)$ and $B(E)$ for the OTBK model ($Z=0.45$, dashed line) and for the SNcNS model ($Z=0.45$, $\gamma_B=0.65$) at $T=0$ (dotted line) and $T=0.96T_c$ (solid line) versus normalized energy. With increasing temperature, the peak at lower energy, reflecting the induced gap, shifts towards $E/\Delta=1$. (b) Calculated SGS with the same parameters as above for the SNcNS model. The voltages corresponding to some of the structures are denoted by arrows.

$\tilde{\gamma}$ equal to zero, the solution in S also becomes independent of x and the Green's functions are determined from^{23,20}

$$-i\epsilon \tan\theta_S = \tilde{\Delta}, \quad (6)$$

$$-i\epsilon \tan\theta_N = \frac{\tilde{\Delta}}{1 + \gamma_B \sqrt{\tilde{\Delta}^2 - \epsilon^2}}, \quad (7)$$

where we have introduced $\gamma_B = \tilde{\gamma}_B d_N / \tilde{\xi}_N$. By inserting the solutions into Eqs. (4) and (5) and employing the OTBK scheme to find the nonequilibrium distribution in the constriction, one can calculate the I - V characteristics.

A remarkable feature of Eq. (7) is the existence of a gap E_g in the density of states $\text{Re}(\cos\theta_N)$ of the N layer, which is obtained from the equation

$$E_g = \frac{\Delta(T)}{1 + \gamma_B \sqrt{\Delta(T)^2 - E_g^2} / \pi k_B T_c}. \quad (8)$$

This gap can be understood to originate from the finite average lifetime of quasiparticles in the thin N layer.²⁰ For $\gamma_B > 0$, the gap is smaller than the gap $\Delta(T)$ in the superconductor at $T < T_c$, but approaches Δ for $T \rightarrow T_c$. This gap in the excitation spectrum of an N layer of finite thickness in proximity to a superconductor has also been obtained by McMillan.⁵ An expression comparable to Eq. (8) for the gap in a quantum well in the clean limit, covered by a superconductor, has been derived by Volkov *et al.*,²⁴ supporting our assumption that the method should yield acceptable results also for the case of an inversion layer. The Andreev reflection probability, which has a single maximum at $E = \Delta$ (for $Z > 0$) in the OTBK model, now reflects the existence of the second, smaller gap by another maximum at $E = E_g$, as can be seen in Fig. 3(a). For $T = 0.96T_c$, both peaks are much closer to each other, because at this temperature the gaps are almost equal in magnitude. Figure 3(b) shows the corresponding calculated dV/dI - V characteristics. Due to the double-peak structure in the Andreev reflection probability, four series of structures are present in this model,⁶ at volt-

ages corresponding to $2\Delta/ne$, $2E_g/ne$, $(\Delta + E_g)/ne$, and $(\Delta - E_g)/ne$. Some of these energy values are marked by arrows in Fig. 3(b). As can be seen, most of the structures are rather weak.

IV. DISCUSSION OF EXPERIMENTAL RESULTS

A. Voltage drop along the interface

A good agreement between the OTBK model and the experimentally found behavior of SSMs systems has been obtained in sandwich-geometry junctions.^{25,26} In coplanar geometry, a much weaker SGS than predicted by the OTBK model or the absence of SGS has been explained by smearing due to a spatially varying voltage drop along the SSM interfaces.^{3,4} The suppression of the SGS might also be caused by the larger effective distance the quasiparticles have to travel in the dissipative region than that between the front edges of the superconducting electrodes due to the voltage distribution under the electrodes. This would lead to a stronger contribution of inelastic scattering, partially relaxing the nonequilibrium distribution. The I - V characteristics then become more similar to that of two SSM junctions in series, for which no SGS is expected.

In Fig. 4, we present the differential resistance at various temperatures of a junction produced before the modification of the sputtering system described in Sec. II. The junction width is $w = 43 \mu\text{m}$, the Nb_2O_5 thickness which corresponds to the electrode separation is $a = 20 \text{ nm}$. At the lowest temperature (1.5 K), the sharp spikes around zero voltage are caused by the jump into the zero-resistance state. Due to the smaller critical currents, this feature is not observable at higher temperatures. Within the broad resistance minimum of full width $\sim 4\Delta/e$, a weak modulation reminiscent of SGS is most clearly visible at 7.1 K, but vanishes for higher and lower temperatures. Using the OTBK model, we estimate $Z \approx 0.6$ from the resistance at zero voltage and $Z \approx 1$ from the magnitude of the excess current, corresponding to transmissivities between 0.74 and 0.50. Of course, this is only a rough estimate, since the dV/dI characteristics are poorly

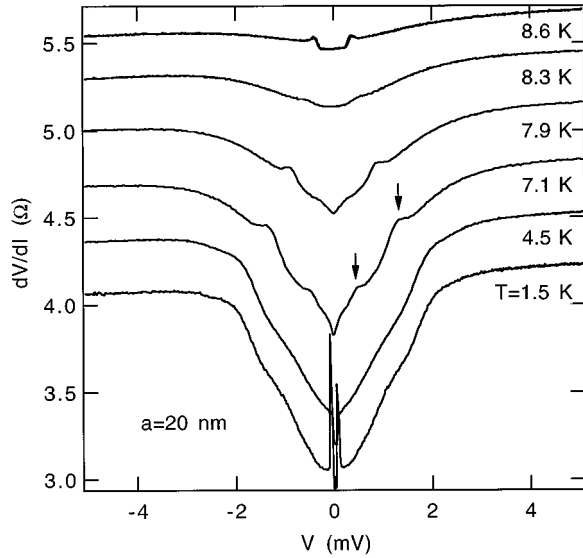


FIG. 4. Differential resistance at various temperatures of a junction with a voltage drop along the SSm interfaces causing smearing of the SGS. Two peaks are visible at intermediate temperatures (see arrows). The curves are successively shifted upwards except for the lowest one for which the resistance scale holds.

described by the OTBK model due to the voltage drop along the interface (see Fig. 5). From the extrapolation of the temperature dependence of the excess current to zero current, we get $T_c = 8.5$ K, which is ~ 0.3 K below the temperature of a sharp drop of the resistance of the whole device when the Nb electrodes become superconducting. This may be explained by only a single superconducting path from the contact pads to the junction being necessary for the resistance drop, but a more or less homogeneous superconducting state at the SSm interface for a detectable excess current. Some deterioration of the Nb near the interface will also contribute. Note the slight asymmetry of the characteristics for positive and negative voltages, which is caused by a current contribution from tunneling through the depletion layer into the degenerate p -type bulk. An asymmetry in the contribution of the tunneling current is expected when the voltage distribution under both electrodes is somewhat different due to different contact quality, which is not unlikely because of the separate depo-

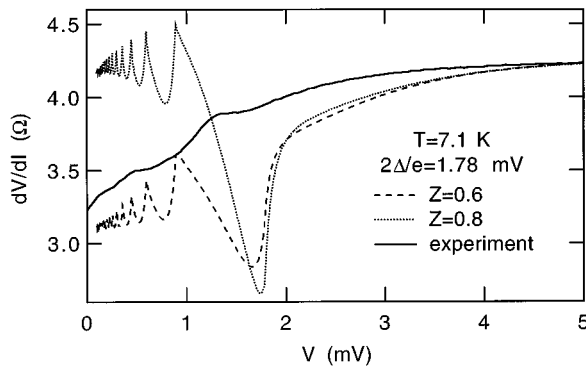


FIG. 5. Differential resistance as in Fig. 4 at 7.1 K (solid line) compared to the result from the OTBK model calculated for $Z=0.6$ (dashed line) and $Z=0.8$ (dotted line) with $R_N=4.3$ Ω and $\Delta(0)=1.39$ meV.

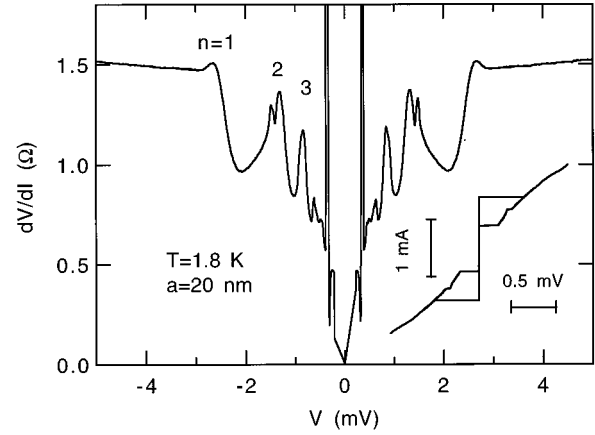


FIG. 6. Differential resistance at 1.8 K of a junction with a high-quality SSm interface. The inset shows the corresponding I - V characteristic in a smaller voltage range with Fiske steps at ± 0.35 mV.

sition of the electrodes. The asymmetry leads to some uncertainty in the determination of the excess current I_{exc} , which otherwise follows closely the temperature dependence of Δ , as expected from the theory.²⁷ The differential resistance at 7.1 K is compared to the OTBK model in Fig. 5. Although there is a considerable contribution of Andreev reflection, as inferred from the resistance decrease for voltages below $\sim 2\Delta/e$, the SGS indicative of *multiple* Andreev scattering is much weaker than in the calculated characteristics. Two further performance parameters supportive of the assumption of a lower-quality Nb/InAs interface, compared to the junctions to be discussed below, are the small $I_c R_N$ product (≈ 100 μ V at 2 K) and $I_{exc} R_N$ product (≈ 320 μ V at 2 K).

B. Proximity-induced coherent state

The dV/dI - V and I - V curve of a junction produced after modification of the sputtering system are shown in Fig. 6. Width and oxide thickness are again $w=43$ μ m and $a=20$ nm. A well developed SGS up to $n=5$ is found. At voltages of ± 0.35 mV, sharp peaks in the dV/dI characteristics are caused by a self-resonance of the ac Josephson effect (Fiske step) in the overlapping part of the Nb electrodes, see Fig. 1. The overlap also leads to a capacitance that is responsible for the hysteresis seen in the inset of Fig. 6.²⁸ This is also observed in the junctions discussed above. It is remarkable that the dV/dI - V characteristics of the junctions with high-quality interfaces are completely symmetric in the examined voltage range up to 9 mV. A critical temperature of $T_c = 8.85$ K is determined from both the extrapolation to zero of the voltage position of the SGS peaks and of I_{exc} . This temperature is again slightly lower than the one of the transition into the nonresistive state of the Nb electrodes. By taking the ratio $\Delta(0)/k_B T_c = 1.9$ for Nb, we obtain the energy gap of the superconductor at $T=0$, $\Delta(0) = 1.45$ meV, which is about 20% too large to account for the position of the SGS at low temperatures in terms of the OTBK model. The discrepancy can be resolved by assuming that the SGS reflects the magnitude of an *induced* gap E_g in the inversion layer under the Nb electrodes. According to Eq. (8), this gap has a magnitude smaller than the superconductor gap Δ , the

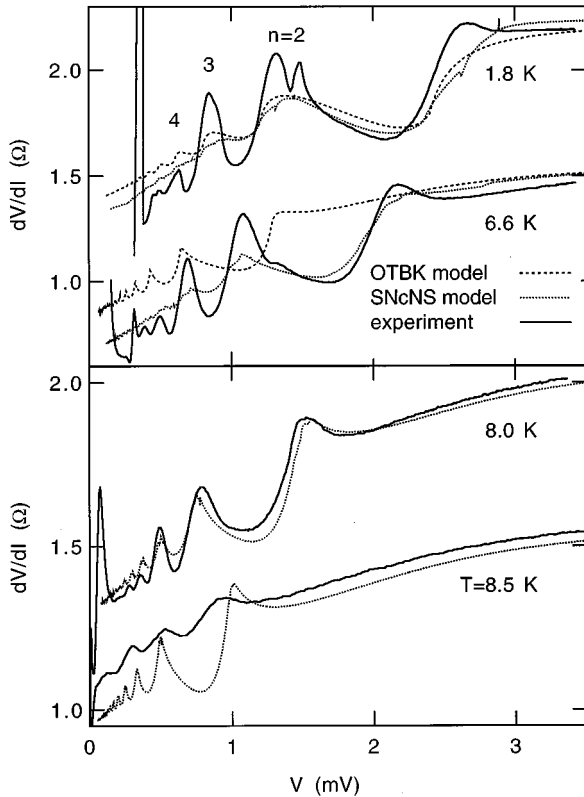


FIG. 7. Comparison of the measured differential resistances (solid line) at four temperatures to the SNcNS model (dotted lines) and the OTBK model (dashed lines). For the SNcNS model, the parameters are $\Delta(0)=1.45$ meV, $R_N=1.55$ Ω , $\gamma_B=0.65$, $Z=0.45$, for the OTBK model, $\Delta(0)=1.20$ meV, $R_N=1.55$ Ω , and $Z=0.45$. The curves for 1.8 and 8.0 K are shifted upwards by 0.7 and 0.5 Ω , respectively.

reduction depending on the barrier transparency parameter γ_B . Nevertheless it tends to zero at the same temperature as Δ . The assumption of an induced gap implies that the complete voltage drop takes place over the 2DEG connecting the two parts of the inversion layer under the Nb electrodes [see Fig. 2(b)]. The parts of the inversion layer covered by the superconductor then remain in thermal equilibrium. Since there is no voltage distribution under the electrodes, smearing effects are absent, explaining the well developed SGS. As long as the inversion layers under both electrodes are in the equilibrium state, any contribution of a tunneling current through the depletion layer will be symmetric in voltage, in agreement with the absence of asymmetry in dV/dI .

In Fig. 7, we compare the dV/dI characteristics calculated from the model of Aminov *et al.*⁶ as described in Sec. III to our experimental data. The parameters for the calculated curves have been slightly changed compared to our preliminary presentation.²⁹ For $T=1.8$ and 6.6 K, we also show the characteristics calculated from the OTBK model, but here we had to assume $T_c=7.32$ K to fit the peak position at the lowest temperature. The normal resistance R_N , equal to the linear slope of the $I-V$ curve at high voltages, increases slightly from about 1.55 to 1.60 Ω in the temperature range of Fig. 7. In the calculation, we used $R_N=1.55$ Ω for all temperatures. From the interface transparency parameter $\gamma_B=0.65$, one finds an induced gap of $E_g=0.81\Delta=1.18$

meV at $T=0$. The barrier strength parameter $Z=0.45$ yields satisfactory agreement between the measurement and the model for the magnitude of the excess current and for the resistance at small voltages at all temperatures. However, at low temperatures the amplitudes of the resistance modulation of the SGS from *both* models are considerably smaller than the experimental ones. A calculated SGS amplitude too small to account for the experiment has also been reported by Kuhlmann *et al.* for Pb/InSb/Pb sandwich junctions.²⁶ Within the OTBK model, an increased amplitude of the SGS would be expected when the Andreev reflection probability dropped more rapidly with increasing energy for $E>\Delta$ than obtained for a steplike variation of the pair potential at the SN interfaces. The reason is that for a smaller above-gap Andreev reflection probability, the condition that the maximum number of subsequent Andreev reflections changes from n to $n+1$ when the voltage drops below $V=2\Delta/ne$ is more ideally fulfilled. The rapid drop in Andreev reflection probability can be caused by a more gradual increase of the pair potential on the superconductor side of the SN interface.³⁰ We have calculated $dV/dI-V$ characteristics in the OTBK model by utilizing the coefficients of Andreev reflection, normal reflection, and transmission obtained by van Son *et al.*³⁰ for a gradual variation of the pair potential. The SGS was indeed increased, compared to the step-function variation.³¹ Although we estimated above that the gap in the superconductors will remain essentially unaffected by the proximity effect, it is well possible that the presence of the 2DEG causes a modification of the proximity-effect induced state in the parts of the inversion layer adjacent to the 2DEG. A calculation within the model of Ref. 6 has not been done so far. Near the critical temperature, the opposite situation occurs, i.e., the calculated SGS is much stronger than the measured one. This may indicate a weakening of the induced coherent state near T_c , so that the effects leading to a smearing of the SGS become more important.

One might wonder whether there should be any barrier at all between the parts of the inversion layer under the Nb and under the oxide, respectively, as it is reflected by the barrier strength parameter $Z=0.45$ given above. Two possible causes for a finite Z are, first, a change in the confining potential of the inversion layer due to different configurations of surface states in the Nb-covered and oxide-covered part and, second, a small contribution of elastic scattering in the channel. In the OTBK and the SNcNS model, elastic scattering in the channel is not included, but similar to an interface barrier it will produce some momentum-reversed quasiparticles, which are responsible for the SGS.

The voltage position of the SGS maxima is plotted versus temperature in Fig. 8. The uppermost solid line represents the temperature dependence of the induced gap, scaled to the $n=1$ peak position at $T=1.8$ K. The other lines are obtained from this curve by multiplying with factors $1/n$, $n=2-5$, demonstrating that the experimentally found peaks are indeed subharmonics. We could equally well have used the superconductor gap for this; it is not meant to show a superior fit by the induced gap. The importance of taking into account the induced gap follows from the discussion of Fig. 7 above. Open and closed symbols in Fig. 8 refer to split peaks. The splitting of the $n=2$ peak and a shoulder of the $n=3$ peak for $T=1.8$ K are clearly visible in Fig. 7. Because

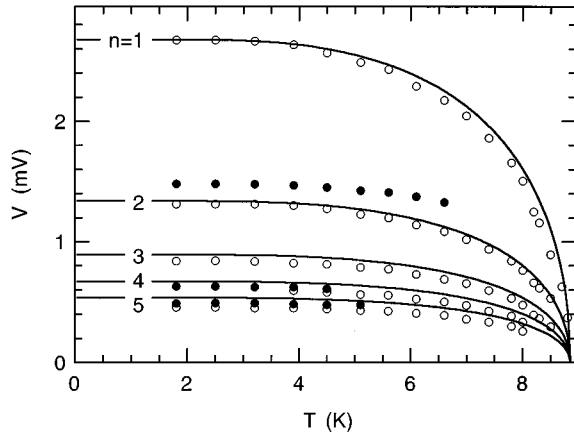


FIG. 8. Voltage positions of the maxima in the differential resistance of the SGS for $n=1-5$ versus temperature. Open and closed symbols refer to split maxima. The solid lines are calculated, the uppermost being $E_g(T)$, scaled to the $n=1$ peak at 1.8 K. The others are subharmonics of this curve.

of its weakness, the latter has not been evaluated in Fig. 8. For $n=4$ and $n=5$, the splitting can be seen in Fig. 9 on an enlarged scale. With increasing temperature, there is a shift of weight from the resistance maximum at higher voltage to the one at lower voltage for these two values of n . For $n=2$ and $n=3$, the maximum at higher voltage and the shoulder disappear when the temperature is raised.

As was discussed in Sec. III, the SNcNS model predicts the appearance of additional series of peaks [see Fig. 3(b)]. In Fig. 7, these are visible in the calculated dV/dI characteristics as small additional structures, which neither in magnitude nor in position correspond to our observation. Probably the appearance of the splitting is strongly influenced by the details of the modification of the energy dependence of the density of states in the N layers, which may deviate from our simple assumptions. However, at the moment we are hesitating to attribute the splitting to this mechanism. Another reason for additional SGS peaks would be differing

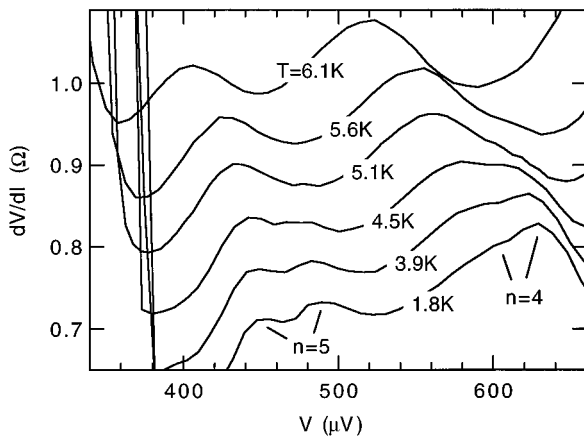


FIG. 9. Low-voltage part of the $dV/dI-V$ characteristics of the junction of Fig. 7, showing the temperature dependence of the splitting of the $n=4$ and $n=5$ peaks. The curves are successively shifted upwards except for the lowest one for which the resistance scale holds.

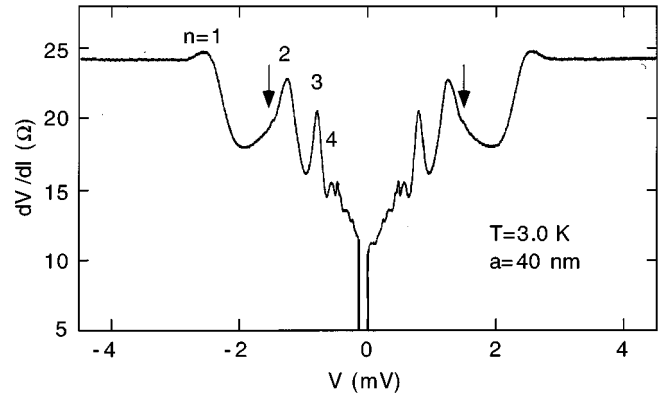


FIG. 10. $dV/dI-V$ characteristic of a junction with $a=40$ nm oxide thickness. The $n=2$ peaks exhibit shoulders (arrows), presumably due to the same effect as the splitting of the peaks in Fig. 7.

magnitudes of the superconducting or induced energy gap for the left and right electrode. From the resistance jump of the electrodes, a difference in critical temperature large enough to account for the observed effect can be excluded. We tried unsuccessfully to find similar structure in the calculated curves by using two different values of γ_B on the two sides. Furthermore, the peculiar temperature-dependent behavior, with nearly no relative shift of the split peaks, could not be explained by such a mechanism.

The shifted position of the SGS peaks at low temperatures indicative of the induced gap, the large modulation compared to the model, and an additional peak corresponding to $n=1$, are common to all junctions with high-quality interfaces. A pronounced splitting has only been observed in the junction discussed above. In the $n=2$ peak of a junction with 40 nm oxide thickness, only a shoulder can be seen in Fig. 10, so that a clear splitting might be limited to very short channel lengths, since other junctions investigated so far had still larger oxide thicknesses up to 80 nm. This remains to be studied in greater detail. The $n=1$ peak already mentioned is neither obtained in the SNcNS nor in the OTBK model at low temperatures, but only appears at higher temperatures (see Fig. 7). It can also be seen at low temperatures in the data of Takayanagi³² and van Huffelen *et al.*²⁵ In both cases, the junctions correspond to the one-dimensional geometry of the OTBK model. It is interesting to note that both the peak splitting and the $n=1$ peak were completely suppressed in a magnetic field of approximately 20 G vertical to the inversion layer. The SGS was clearly reduced in magnitude but still present. Parallel to the inversion layer, fields of ~ 2000 G were necessary to produce the same effect.

Figure 8 further shows that heating effects are negligible over the whole voltage range of the SGS. Heating would be expected to shift the position of the SGS peaks to lower voltage at intermediate temperatures, thus causing an appreciable deviation from the temperature dependence of the gap.^{33,25} The strongest shift would be expected for the peaks at the highest voltages, where heating effects are strongest. A small deviation of the peak position from the temperature dependence of E_g is also obtained for the calculated SGS. Due to the existence of different series of peaks in the calculated curves, we did not compare our data to theoretical peak positions.

The normal resistance of the junction is obtained from the theory as $R_N = (1 + 2Z^2)R_{Sh}$, with the Sharvin resistance³⁴ $R_{Sh} = (h/2e^2)\pi/k_F w$ for a 2DEG. Estimating a carrier density of $N_{s,0} = 1.5 \times 10^{16} \text{ m}^{-2}$ in the lowest subband,³⁵ we find $R_{Sh} \approx 3.1 \Omega$ and $R_N \approx 4.4 \Omega$. Shunting by tunneling into the bulk and by the inversion layer next to the junction, as well as contributions from higher subbands, are not taken into account. Considering the uncertainties, the above value is in reasonable agreement with the measured $R_N = 1.55 \Omega$, so that the notion that the complete voltage drops over the 2DEG seems justified. The trace shown in Fig. 10 has been recorded for the junction with the highest resistance $R_N = 24 \Omega$ found so far, a value that can be caused by a smaller effective width of the junction due to some variation of the interface quality over the width. The nominal width is $43 \mu\text{m}$ as for the junction with $R_N = 1.55 \Omega$. The assumption of a partly reduced interface quality in junctions with higher normal resistance is supported by a scaling of the $I_c R_N$ and $I_{exc} R_N$ of the junctions with the normal resistance; the values are between $I_c R_N = 1.3 \text{ mV}$ and 0.7 mV and $I_{exc} R_N = 1.9 \text{ mV}$ and 1.1 mV , respectively, for the junction with $R_N = 1.55 \Omega$ and 24Ω . All values are considerably larger than those for the junctions showing smearing effects. The small temperature dependence of R_N noted above can have various reasons. For example, a small contribution of scattering, with a temperature-dependent scattering length, may explain this effect. Also a weakening of the induced coherent state with some extension of the voltage drop under the electrodes at higher temperatures may be responsible, which has already been discussed above as a cause for the decrease of the SGS amplitude at temperatures near T_c .

V. CONCLUSIONS

We have compared the I - V characteristics of coplanar Nb/ p -type InAs(2DEG)/Nb junctions with different SSm interface qualities. For lower interface quality, we found signatures of a voltage drop occurring in the inversion layer under

the Nb electrodes. For high interface quality, the absence of smearing and the shifted position of the SGS with respect to the expectation from the OTBK model² can be understood by assuming that the electron system in the inversion layer under the Nb electrodes is strongly influenced by the proximity effect. This has been taken into account in a recent theory of Aminov *et al.*⁶ As a result of the presence of the superconductor, a gap opens in the density of states of the inversion layer. This gap is comparable in magnitude to the energy gap of the superconductor for highly transmissive interfaces, because the inversion layer is so thin. The application of this theory to our junctions implies that the voltage drops completely over the 2DEG under the oxide. This can also explain why smearing effects are absent despite of the coplanar geometry. The gap induced in the density of states of the inversion layer causes the observed shift of the SGS. The shift, the large amplitude, and the presence of the $n=1$ peak at low temperatures are common to all contacts with good interfaces. We also discussed the observation of a splitting of the SGS, the origin of which could not be finally resolved. It should be kept in mind that due to our simplifying assumptions, a detailed agreement between the model and the experiment cannot be expected. We further want to point out that the differences between the performance data $I_c R_N$, $I_{exc} R_N$, and barrier transmissivity obtained for the two types of junction characteristics discussed are quite small, regarding the vastly different qualitative appearance of the dV/dI characteristics that has been demonstrated above. On the one hand, this again underlines the high sensitivity to interface quality of SSm junctions. On the other hand, it suggests that under certain conditions, the voltage drop might easily extend somewhat under the electrodes also in the junctions with good interfaces, as has been discussed above for the case of higher temperatures.

ACKNOWLEDGMENTS

We thank Th. Wiegner and F. Herrmann for the XPS analysis and A. A. Golubov for helpful discussions.

- ¹A. F. Andreev, Zh. Eksp. Teor. Fiz. **46**, 1823 (1964) [Sov. Phys. JETP **19**, 1228 (1964)].
- ²M. Octavio, M. Tinkham, G. E. Blonder, and T. M. Klapwijk, Phys. Rev. B **27**, 6739 (1983).
- ³A. W. Kleinsasser, T. N. Jackson, D. McInturff, F. Rammo, G. D. Pettit, and J. M. Woodall, Appl. Phys. Lett. **57**, 1811 (1990).
- ⁴J. Nitta, T. Akazaki, H. Takayanagi, and K. Arai, Phys. Rev. B **46**, 14 286 (1992).
- ⁵W. L. McMillan, Phys. Rev. **175**, 537 (1968).
- ⁶B. A. Aminov, A. A. Golubov, and M. Yu. Kupriyanov, Phys. Rev. B **53**, 365 (1996).
- ⁷H. Kroger, L. N. Smith, and D. W. Jillie, Appl. Phys. Lett. **39**, 280 (1981).
- ⁸P. Kofstad, *Nonstoichiometry, Diffusion, and Electrical Conductivity in Binary Metal Oxides* (Wiley, New York, 1972).
- ⁹J. K. Hulm, C. K. Jones, R. A. Hein, and J. W. Gibson, J. Low Temp. Phys. **7**, 291 (1972).
- ¹⁰M. Grundner and J. Halbritter, J. Appl. Phys. **51**, 397 (1980).
- ¹¹R. B. Laibowitz and J. J. Cuomo, J. Appl. Phys. **41**, 2748 (1970).
- ¹²J. Aponte, E. Rivera, A. Sa Neto, and M. Octavio, J. Appl. Phys. **62**, 700 (1987).
- ¹³A. Chrestin, T. Matsuyama, and U. Merkt, in *23rd International Conference on the Physics of Semiconductors*, edited by Matthias Scheffler and Roland Zimmermann (World Scientific, Singapore, 1996), Vol. 4, 3403.
- ¹⁴T. M. Klapwijk, G. E. Blonder, and M. Tinkham, Physica **109&110B**, 1657 (1982).
- ¹⁵G. E. Blonder, M. Tinkham, and T. M. Klapwijk, Phys. Rev. B **25**, 4515 (1982).
- ¹⁶G. M. Eliashberg, Zh. Eksp. Teor. Fiz. **61**, 1254 (1971) [Sov. Phys. JETP **34**, 668 (1971)].
- ¹⁷A. I. Larkin and Yu. N. Ovchinnikov, Zh. Eksp. Teor. Fiz. **68**, 1915 (1975) [Sov. Phys. JETP **41**, 960 (1976)].
- ¹⁸M. Yu. Kupriyanov and V. F. Lukichev, Zh. Eksp. Teor. Fiz. **94**, 139 (1988) [Sov. Phys. JETP **67**, 1163 (1988)].
- ¹⁹A. A. Golubov and M. Yu. Kupriyanov, Pis'ma Zh. Eksp. Teor. Fiz. **61**, 830 (1995) [JETP Lett. **61**, 850 (1995)].
- ²⁰A. A. Golubov and M. Yu. Kupriyanov, Physica C **259**, 27 (1996).

- ²¹A. F. Mayadas, R. B. Laibowitz, and J. J. Cuomo, *J. Appl. Phys.* **43**, 1287 (1972).
- ²²T. Matsuyama, Ph.D. thesis, Shaker, Aachen, 1994.
- ²³A. A. Golubov, E. P. Houwman, J. G. Gijbertsen, V. M. Krasnov, J. Flokstra, H. Rogalla, and M. Yu. Kupriyanov, *Phys. Rev. B* **51**, 1073 (1995).
- ²⁴A.F. Volkov, P.H.C. Magnée, B.J. van Wees, and T.M. Klapwijk, *Physica C* **242**, 261 (1995).
- ²⁵W. M. van Huffelen, T. M. Klapwijk, D. R. Heslinga, M. J. de Boer, and N. van der Post, *Phys. Rev. B* **47**, 5170 (1993).
- ²⁶M. Kuhlmann, U. Zimmermann, D. Dikin, S. Abens, K. Keck, and V. M. Dmitriev, *Z. Phys. B* **96**, 13 (1994).
- ²⁷A. W. Kleinsasser, *Appl. Phys. Lett.* **62**, 193 (1993).
- ²⁸W. C. Stewart, *Appl. Phys. Lett.* **12**, 277 (1968); D. E. McCumber, *J. Appl. Phys.* **39**, 3113 (1968).
- ²⁹A. Chrestin, K. Biedermann, T. Matsuyama, and U. Merkt, *Czech. J. Phys.* **46**, Suppl. S4, 2315 (1996).
- ³⁰P. C. van Son, H. van Kempen, and P. Wyder, *Phys. Rev. B* **37**, 5015 (1988).
- ³¹A. Chrestin, Ph.D. thesis, Shaker, Aachen, 1997.
- ³²H. Takayanagi, *Physica B* **218**, 113 (1996).
- ³³M. Octavio, W. J. Skocpol, and M. Tinkham, *IEEE Trans. Magn.* **MAG-13**, 739 (1977).
- ³⁴Yu. V. Sharvin, *Zh. Eksp. Teor. Fiz.* **48**, 984 (1965) [*Sov. Phys. JETP* **21**, 655 (1965)].
- ³⁵R. Scharnweber, T. Matsuyama, and U. Merkt, *Supercond. Sci. Technol.* **7**, 141 (1994).